Developmental and Degenerative Cardiac Defects in the Taiwanese Mouse Model of Severe Spinal Muscular Atrophy

Gillian K. Maxwell[1], *Eva Szunyogova*[1,3], *Hannah K. Shorrock*[2,3], *Thomas H. Gillingwater*[2,3] *and Simon H. Parson*[1,3]

[1]Institute for Medical Science, University of Aberdeen, Aberdeen, Scotland, AB25 2ZD
[2]Edinburgh Medical School: Biomedical Sciences, University of Edinburgh, Edinburgh, Scotland, EH8 9AG
[3]Euan MacDonald Centre for Motor Neurone Disease Research, University of Edinburgh, Edinburgh, Scotland, EH16 4SB

Running title: Heart Defects in SMA

Key words: Cardiovascular, cardiac, stress, cell death, ventricle, septum

Abstract

Spinal muscular atrophy (SMA), an autosomal recessive disease caused by a decrease in levels of the Survival Motor Neuron (SMN) protein, is the most common genetic cause of infant mortality. Although neuromuscular pathology is the most severe feature of SMA, other organs and tissues, including the heart, are also known to be affected in both patients and animal models. Here, we provide new insights into changes occurring in the heart, predominantly at pre- and early-symptomatic ages, in the Taiwanese mouse model of severe SMA. Thinning of the interventricular septum and dilation of the ventricles occurred at pre- and early-symptomatic ages. However, the left ventricular wall was significantly thinner in SMA mice from birth, occurring prior to any overt neuromuscular symptoms. Alterations in collagen IV protein from birth indicated changes to the basement membrane and contributed to the abnormal arrangement of cardiomyocytes in SMA hearts. This raises the possibility that developmental defects, occurring prenatally, may contribute to cardiac pathology in SMA. In addition, cardiomyocytes in SMA hearts exhibited oxidative stress at pre-symptomatic ages and increased apoptosis during early-symptomatic stages of disease. Heart microvasculature was similarly decreased at an early-symptomatic age, likely contributing to the oxidative stress and apoptosis phenotypes observed. Finally, an increased incidence of blood retention in SMA hearts post-fixation suggests the likelihood of functional defects, resulting in blood pooling. These pathologies mirror dilated cardiomyopathy, with clear consequences for heart function that would likely contribute to potential heart failure. Our findings add significant additional experimental evidence in support of the requirement to develop systemic therapies for SMA capable of treating non-neuromuscular pathologies.

Introduction

Our understanding of the pathogenesis of spinal muscular atrophy (SMA) remains incomplete, despite its classification as a single gene disorder and a major genetic cause of infant mortality. The ubiquitously expressed Survival Motor Neurone protein (SMN) – named due to the predominant motor neurone loss seen in SMA (Werdnig, 1891; Hoffmann, 1892) – is produced from two genes in humans, with the majority of full-length protein produced by the *SMN1* gene (Lorson *et al.,* 1999). In SMA, an autosomal recessive disease, mutations in the *SMN1* gene leave the *SMN2* gene alone to produce small amounts of full-length, functional SMN protein (Lefebvre *et al.,* 1995). This is sufficient to prevent embryonic lethality but results in the pathology of SMA.

SMA is primarily characterised by loss of α-motor neurones in the spinal cord, causing denervation and resulting atrophy of skeletal muscle (Lunn and Wang, 2008; Powis *et al.,* 2016a). However, a range of non-neuromuscular pathologies are also now apparent (reviewed in: Hamilton and Gillingwater, 2013; Shababi *et al.,* 2014; Nash *et al.,* 2016), including abnormalities affecting the liver (Vitte *et al.,* 2004; Szunyogova *et al.,* 2016), lung (Schreml *et al.,* 2012), pancreas (Bowerman *et al.,* 2012; Bowerman *et al.,* 2014), spleen (Thomson *et al.,* 2016; Deguise *et al.,* 2017; Khairallah *et al.,* 2017), testis (Ottesen *et al.,* 2016), intestines (Sintusek et al., 2016) and the vascular system (Shababi *et al.,* 2012;

Somers *et al.,* 2012; Sintusek *et al.,* 2016; Somers *et al.,* 2016). Amongst these, cardiac abnormalities were first putatively described in SMA patients ~60 years ago (Sterne and Lavieuville, 1964; Gardner-Medwin *et al.,* 1967), but are only now becoming accepted as a potentially core aspect of SMA, particularly in severe forms of the disease (Wijngaarde *et al.,* 2017).

In patients, cardiac defects have been described across mild and severe forms of SMA, commonly falling into two major categories: structural defects and arrhythmias. Congenital heart defects, including atrial septal defects, ventricular septal defects and hypoplastic aortic arch, are the most common structural defects observed in SMA patients (Møller *et al.,* 1990; Burglen *et al.,* 1995; Mulleners *et al.,* 1996; Jong *et al.,* 1998; El-Matary *et al.,* 2004; Cook *et al.,* 2006; Sarnat and Trevenen *et al.,* 2007; Vaidla *et al.,* 2007; Menke *et al.,* 2008; Araujo *et al.,* 2009; Grotto *et al.,* 2016; Krupickova *et al.,* 2017). However, pulmonary hypertension, ventricular enlargement, systolic murmurs and cardiomyopathies have also been reported (Tanaka *et al.,* 1976; Tanaka *et al.,* 1977; Kimura *et al.,* 1980; Møller *et al.,* 1990; Distefano *et al.,* 1994; Elkohen *et al.,* 1996; Finsterer *et al.,* 1999; El-Matary *et al.,* 2004; Collado-Ortiz *et al.,* 2007; Vaidla *et al.,* 2007; Menke *et al.,* 2008; Kuru *et al.,* 2009). In the case of arrhythmias, bradycardias are most predominant in children with SMA, although heart block and ECG tremors have also been noted (Tanaka *et al.,* 1976; Kimura *et al.,* 1980; Dawood and Moosa, 1983; Coletta *et al.,* 1989; Finsterer *et al.,* 1999; Arai *et al.,* 2005; Hachiya *et al.,* 2005; Takahashi *et al.,* 2006; Rudnik-Schöneborn *et al.,* 2008; Roos *et al.,* 2009; Haliloglu *et al.,* 2015; Grotto *et al.,* 2016). Together these findings do not immediately suggest a common or consistent aetiology. Therefore, further work is required to understand the degree to which these represent primary or secondary causative co-morbidities.

Heart defects have been reliably reproduced in both severe and mild mouse models of SMA. These include; structural changes represented by thinning of the interventricular septum (IVS) and left ventricular (LV) wall (Bogdanik *et al.,* 2015; Schreml *et al.,* 2013; Shababi *et al.,* 2010); dilated cardiomyopathy (Bevan *et al.,* 2010; Heier *et al.,* 2010; Schreml *et al.,* 2013; Bogdanik *et al.,* 2015); and increased fibrosis and oxidative stress (Shababi *et al.,* 2010). In both severe and mild mouse models, reports of both a decreased ejection fraction (Bevan *et al.,* 2010; Bogdanik *et al.,* 2015) and arrhythmias, particularly bradycardia (Bevan *et al.,* 2010; Heier *et al.,* 2010; Shababi *et al.,* 2010; Biondi *et al.,* 2012; Bogdanik *et al.,* 2015), indicate functional changes. Significantly, in the very mild 'Burgheron' mouse model, some mice die from severe cardiomyopathy rather than the effects of neuromuscular pathology (Bogdanik *et al.,* 2015). However, our understanding of these heart defects is still incomplete.

Heart defects in SMA represent only one aspect of disruption to the cardiovascular system. Other notable changes include a pronounced decrease in blood vessel density in skeletal muscle of both patients and a severe mouse model (Somers *et al.,* 2012; Somers *et al.,* 2016), and in the spinal cord (Somers *et al.,* 2016), intestines (Sintusek *et al.,* 2016) and heart (Shababi *et al.,* 2012) of severe SMA mouse models. Distal necrosis is seen in the fingers and toes of patients (Araujo *et al.,* 2009; Rudnik-Schöneborn *et al.,* 2010), and in the ears and tail of mouse models (Hsieh-Li *et al.,* 2000; Tsai *et al.,* 2006; Narver *et al.,* 2008; Hua *et al.,* 2010; Riessland *et al.,* 2010; Schreml *et al.,* 2013; Bogdanik *et al.,* 2015; Catapano

et al., 2016). This necrosis in patients is resolved by anticoagulant treatment, suggesting that these are thrombotic occlusions (Araujo *et al.,* 2009). Finally, there is consistent evidence of persistent extramedullary haematopoiesis in SMA. In a severe mouse model, the liver is undergoing erythropoiesis; it has an increased number of megakaryocytes; elevated platelet levels; and higher levels of normoblasts (nucleated red blood cells) in blood samples (Szunyogova *et al.,* 2016). Similarly, the spleen of a severe SMA mouse also has increased megakaryocyte density and immature architecture indicative of ongoing haematopoiesis (Thomson *et al.,* 2016). Abnormalities of the spleen have also been reported in SMA patients, with red pulp congestion and the presence of erythroid precursors (Thomson *et al.,* 2016).

Given the growing awareness of cardiovascular defects in SMA, we set out to undertake a detailed morphological assessment of the heart in the 'Taiwanese' mouse model of severe SMA. By focussing on the period between birth and the first appearance of overt neuromuscular symptoms, we attempted to identify the initiation of cardiovascular defects, giving a better understanding of mechanisms underlying these phenotypes in SMA.

We report significant structural and molecular defects in the heart, prior to, or in tandem with overt neuromuscular pathology; key molecular targets of SMN-depletion in the heart; and suggest a multifactorial cardiovascular system pathology.

Methods

Mice

The Taiwanese SMA mouse model on a congenic FVB background was used to replicate a severe phenotype of SMA. Taiwanese SMA mice were maintained as breeding pairs under standard specific-pathogen-free conditions in animal care facilities at Edinburgh University (Hsieh-Li *et al.,* 2000; Riessland *et al.,* 2010; Powis *et al.,* 2016b). Offspring littermates were either heterozygous for Smn knockout ($Smn^{+/-};SMN2^{tg/0}$) and used as controls, or homozygous ($Smn^{-/-};SMN2^{tg/0}$) and used as SMA disease model. All experimental protocols were approved by Edinburgh University internal research and ethics committees and were carried out in accordance with licenses obtained from the United Kingdom Home Office under the Animals (Scientific Procedures) Act 1986. Genotyping of mice was carried out *via* standard PCR protocols (Wishart *et al.,* 2014). Day of birth is defined as postnatal day 1 (P1).

Tissue Processing

Hearts were harvested between P1-P8 from mice sacrificed by intraperitoneal injection of sodium pentobarbital in accordance with UK guidance and rules for the use of animals in research. Hearts were then fixed for 4hrs in 4 % paraformaldehyde (PFA) before undergoing cryoprotection in 30 % sucrose and embedding in OCT. Hearts were cryo-sectioned at a thickness of 7 µm. Sections then underwent either basic haematoxylin and eosin (H&E) staining or immunohistochemistry.

Immunohistochemisty

Heart sections were incubated overnight at 4 °C with the following primary antibodies: rabbit polyclonal anti-Collagen IV (Millipore, AB756P), rabbit polyclonal anti-Ki67 (Abcam, ab16667) and rat monoclonal anti-Ly76 (Abcam, ab91113); and for 2 hours with the corresponding secondary antibodies: Cy3 Goat anti-rabbit IgG (H+L) (Life Technologies, A-10520) and Cy3 goat anti-rat IgG (H+L) (Life Technologies, A-10522). 3x10 minute washes in PBT (0.1M PBS with 0.1 % Tween-20) and 0.1 M PBS were carried out between and after antibody incubation. Rhodamine labelled Griffonia Lectin 1 (GSL-1) was used to stain vasculature. Sections were coverslipped using mowiol mounting media (10% Mowiol (Sigma-Aldrich, 81381), 20 % Glycerol, 50 % 0.2 M Tris buffer pH 8.5, 3 % 1,4-diazobicyclooctane made up in distilled water) containing DAPI. Sections were imaged using Nikon eclipse e400 microscope (10x objective) and its images captured using QICAM Fast 1394 camera and Improvision Velocity 4 image capture software.

Quantitative Western Blotting

Quantitative Western blotting was carried out on 3 hearts per genotype (Eaton *et al.,* 2014). Briefly, hearts were digested in RIPA buffer containing 2.5 % Halt protease inhibitor cocktail and homogenised. BCA assay was carried out to quantify protein concentration of individual samples. 15 µg of protein was loaded per well. Samples were separated by electrophoresis on precast Bolt™ 4-12 % Bis-Tris Plus Gels (NW04120BOX) and then transferred to nitrocellulose membranes using semi-dry I-Blot® transfer system (Invitrogen, UK). Reversible total protein stain was carried out using Li-COR Revert total protein stain and wash solution (LI-COR, 926-11011). To revert the membrane 0.1 % sodium hydroxide in 30 % methanol in water was used. Membranes were incubated overnight at 4 °C with the following primary antibodies: rabbit polyclonal anti-caspase-3 (Abcam, ab13847), rabbit polyclonal anti-angiotensin II receptor 1 (AT-1) (Abcam, ab18801) and goat polyclonal anti-platelet endothelial cell adhesion molecule-1 (PECAM-1) (R&D Systems, AF3628); diluted in SeaBlock blocking buffer (ThermoFisher Scientific, 37527) with Tween-20. Corresponding secondary antibodies, donkey anti-rabbit Alexa Fluor® 680 IgG (H+L) (Abcam, ab186692) and donkey anti-goat Alexa Fluor® 790 IgG (H+L) (Abcam, ab175784), were incubated at room temperature for 2 hours. 6x10 minute washes with 0.1 M PBS were carried out between and after antibody incubation. Membranes were imaged using Li-COR Odyssey Scanner and Software. Due to alterations in the expression levels of many standard loading control proteins in SMA tissues, total protein was used to normalise protein expression (Eaton et al., 2013). Image Studio Lite was used for quantification of Western blots.

Heart Quantification

In all analyses, folded or damaged heart sections were rejected. ImageJ was used to measure the area of the heart and ventricles, for cell counts, and for red blood cell density analysis. A protractor generated in Adobe Photoshop was used to quantify IVS and LV walls.

Quantification of Structural Changes to the Heart: IVS width, LV wall width and ventricular lumen area were measured from 4 H&E stained slides, containing ~8 heart sections per heart (~30 in total per heart), from the same relative area, i.e. between the apex and the atrioventricular septum. Images were captured at 40x magnification and under the same

exposure. The freehand selection tool in Image J was used to measure the area of the heart and the left and right ventricles in calibrated images. In Adobe Photoshop, to measure the IVS and the LV wall, the largest rectangle of best fit was placed in the LV and the centre was found. From here, lines of 20^{o} were drawn radially to intersect the IVS or LV wall and the ruler tool was used to measure between points on these lines. Distance was either measured between the edge of the two ventricles for IVS width or between the left ventricle wall and the edge of the heart for LV wall width.

Ly76 Density Quantification: The density of Ly76 positive cells was measured from ~8 sections taken from the same relative area in each heart. Images were captured at 40x magnification and under the same exposure. Brightness and contrast were enhanced in Adobe Photoshop. The enhanced images were then converted into binary in ImageJ, where Ly76 positive cells were assigned black, and the background white. A ratio of black to white pixels for the whole heart area could then be calculated, allowing a relative value for Ly76 positive cell area relative to heart area, expressed as a percentage.

Cell Density and Ki67 Positive Cell Quantification: Cell density was calculated from ~8 sections at the same relative area in each heart. From each heart section 6 different images at 400x magnification were captured fully composed of tissue at the same exposure, from the same 6 areas for each heart, i.e. in the LV wall, the IVS and the RV wall. DAPI-blue channels and Ki67-red channels were merged in Adobe Photoshop. ImageJ was then used to count the number of DAPI positive nuclei only, and both DAPI and Ki67 positive nuclei combined in the field of view. The number of Ki67 and DAPI positive cells combined was expressed as a percentage of total number of DAPI positive cells.

Statistics: All experimental groups consisted of a minimum of 3 different animals, which has previously shown to be sufficient to attain statistical significance (Szunyogova *et al.,* 2016). All graphs are shown as mean ± SEM. Unpaired two-tailed t-test and two-way ANOVA were carried out using PRISM, where * < p0.05; ** < p0.01; *** < p0.001.

Results

Gross Heart Morphology is Altered in SMA Mice

Initial assessment of hearts from SMA mice revealed no obvious gross anatomical disorganisation across all ages studied from P1 and P3 (pre-symptomatic), through P5 (early symptomatic) and P8 (symptomatic), but SMA hearts were smaller when compared to control (Fig. 1A). When heart weight was expressed relative to body weight (which is lower in late symptomatic SMA mice; see Powis *et al*., 2016b), there was no significant difference between SMA and control hearts at any of the ages examined (P1,3,5,8: ns > 0.05: Fig. 1B). Upon closer observation of transverse sections of the heart stained with H&E, SMA hearts appeared to have thinner ventricular walls, and larger ventricles, which were congested with blood (Fig. 1C). IVS and LV wall measurements have been made previously (Bevan *et al.,* 2010; Shababi *et al.,* 2010), however, the time course of ventricle dilation has not been analysed. Quantification revealed that the relative area of the heart comprised of the ventricles was significantly greater in SMA, at pre (P3) and early (P5) -symptomatic ages

suggesting enlargement of the ventricles occurs early in the SMA phenotype (P1: ns > 0.05; P3: *** <0.001; P5: * < 0.05) (Fig. 1D). Furthermore, the IVS and LV wall, which together comprise the main muscle mass of the heart, were thinner, relative to body weight, in SMA hearts from an early age (Fig. 1E and 1F). The IVS was significantly thinner at pre and early-symptomatic ages (P1: ns > 0.05; P3: * < 0.05; P5: ** < 0.01), whereas the LV wall was significantly thinner from birth onwards (P1: * < 0.05; P3: *** < 0.001; P5: * < 0.05).

These data not only show significant changes in the heart wall and IVS in the Taiwanese SMA mouse model, but moreover indicate that they develop in pre-symptomatic animals, with evidence of cardiac defects present at birth. This suggests that heart pathology is likely to represent a primary event in SMA, and is not simply a secondary consequence of neuromuscular pathology.

Cardiomyocytes are Disorganised in the SMA Heart

Given the gross pathology evident in the heart wall of SMA mice, we next investigated the fine structure of the heart to determine the likely aetiology of the defects in the IVS and LV wall. To determine the arrangement of cardiomyocytes, collagen IV immunohistochemistry was used to highlight surrounding basement membranes from birth to early-symptomatic ages (P1, P3 and P5). The basement membrane surrounds the cardiomyocytes providing structural support and is important during heart development for the formation of sarcomeres.

At P5 the LV wall in control hearts was clearly formed by 3 layers of cardiac muscle; superficial oblique, cylindrical middle, and deep longitudinal layers (Fig. 2A v and 2B i). The middle layer in particular was most pronounced, containing strands of cardiomyocytes which spiralled out anti-clockwise from the LV, twisting in the orientation of heart contraction (Greenbaum *et al.,* 1981; Sedmera and McQuinn, 2009). This structure not only ensures a coherent electrical impulse transfer, but is essential for the twisting motion of the ventricles observed during contraction of the heart. At birth, this spiral structure surrounding the LV was beginning to develop in the control heart (Fig. 2A i). In contrast, the heart wall in SMA was disorganised with no apparent development of cardiomyocyte orientation between birth and P5 (Fig. 2A ii, 2A iv, 2A vi and 2B ii). The appearance was in fact similar to an embryonic heart, where muscle is arranged circumferentially around the ventricle rather than radiating from it (Sedmera and McQuinn, 2009).

During embryonic development trabeculations are formed in the ventricles prior to the formation of the coronary vasculature to increase surface area for nutrient uptake (Sedmera *et al.*, 2000). An essential stage in increasing the mass of the compact muscular wall of the heart is compaction of these trabeculae, which coincides with the formation of the coronary blood supply (Sedmera *et al.*, 2000). In the control heart, nearer the luminal wall of the LV, trabeculations can often be seen. These trabeculations are sparse, do not penetrate far into the lumen, and appear large enough to allow the growth of a blood supply to these cells

(Fig. 2B iii). In SMA, these trabeculations were greater in number, projected further into the lumen, and were very thin, with little capacity for a blood supply to invade (Fig. 2B iv). This occured from birth, where P1 SMA hearts had little definition between the compact wall and the ventricles (Fig. 2A ii) and was still present at early-symptomatic (P5) ages (Fig. 2A vi).

Collagen IV immunostaining, used to visualise cardiomyocyte arrangement, showed a non-uniform pattern of labelling with an apparent decrease in staining, particularly towards the superficial surface in the SMA hearts compared to control hearts. This suggests a defect in the basement membrane, of which collagen IV is a key component and which is essential to maintain the organisation of cardiomyocytes in the heart. Further, a significant global decrease in collagen IV expression in SMA hearts was demonstrated by quantitative Western blotting at birth (P1: *<0.05) (Fig. 2C). Importantly, collagen IV interacts directly with SMN protein (Fuller *et al.,* 2016), suggesting a potential mechanistic link between SMN depletion and heart wall disorganisation.

SMA Hearts Have a Decreased Number of Cardiomyocytes Associated with Increased Apoptosis

To establish the cellular basis of the changes in SMA heart structure, cardiomyocytes were specifically investigated from birth (P1) through to early-symptomatic ages (P5). SMA hearts showed a significant decrease in cardiomyocyte number per unit area (density) at pre- (P3) and early- (P5) symptomatic ages but not at birth (P1: ns > 0.05; P3: **<0.01; P5: ***< 0.001) (Fig 3B). To establish the nature of this decrease in cardiomyocyte density, cell proliferation and apoptosis were analysed. Heart sections were stained with Ki67 (Fig. 3A), a proliferation marker expressed during all phases of division (Scholzen and Gerdes, 2000), however, no significant difference in the number of proliferating cells between control and SMA was observed between birth and P5 (P1: ns > 0.05; P3: ns > 0.05; P5: ns > 0.05) (Fig 3C). Apoptosis was analysed by Western blot for caspase-3, involved in the activation cascade of caspases responsible for apoptosis execution (Porter and Jänicke, 1999), which showed a significant increase in early-symptomatic SMA hearts (P1: ns > 0.05; P3: ns > 0.05; P5: **< 0.01) (Fig. 3D). This suggests that the decrease in cardiomyocyte density may be linked to an increase in cell death consistent with atrophy of the heart.

Oxidative Stress is Present in SMA Hearts

Increased apoptosis in cardiomyocytes was investigated further by examining a common trigger: oxidative stress, which is present in Δ7 SMA mice exhibiting a neuromuscular phenotype (Shababi *et al.,* 2010). We analysed angiotensin II receptor 1 (AT1) levels as a marker of oxidative stress in the heart, as this increases ROS by elevating the activity of NADPH oxidase during heart failure (Qin *et al.,* 2005). Immunohistochemistry showed dramatically increased amounts of AT-1 in the SMA heart at birth compared to the control heart (Fig4A). Western blot analyses confirmed these higher levels of AT-1 in SMA compared to control hearts at both P3 and P5 (P1: ns > 0.05; P3: *< 0.05; P5: ** < 0.01) (Fig. 4A), indicating the presence of oxidative stress in SMA hearts with onset at a pre-symptomatic age.

To substantiate this finding we looked for evidence of mitochondrial-derived oxidative stress as multiple proteins in the mitochondria are associated with increased ROS production (Martínez-Reyes and Cuezva, 2014). This includes the ATP synthase complex, which interacts directly with SMN (Fuller *et al.,* 2016). We analysed levels of subunit 6 of the ATP synthase complex as mutations or overexpression of this subunit are particularly associated with oxidative stress (Manczak *et al.,* 2005; Jonckheere *et al.,* 2012). Western blot analyses showed significantly higher levels of MT-ATP6 in SMA at birth compared to controls (P1: *<0.05) (Fig. 4B).

The presence of increased oxidative stress at birth not only suggests this is an important event in the aetiology of SMA heart pathology, but is also indicative of early mitochondrial dysfunction. As oxidative stress is present prior to increased caspase-3 expression, and significantly occurs prior to the appearance of neuromuscular symptoms, it is likely to precede and contribute to cardiomyocyte apoptosis and heart dysfunction.

SMA Heart Microvasculature is Significantly Decreased

A reduction in capillary density has been reported across multiple tissues in SMA patients and animal models, where it is associated with tissue hypoxia (Somers *et al.,* 2016). Previously, decreased microvasculature in the heart of the Δ7 SMA mouse model has only been studied at a late-symptomatic age. Here, microvasculature was analysed at early- and pre-symptomatic ages to establish if it might contribute to, rather than be a symptom of, heart pathology. Immunostaining of hearts with GSL-1 endothelial cell marker indicated a gross decrease in microvasculature density throughout the heart wall particularly at P5 in SMA (Fig 5A,B). Western blot for a second endothelial cell marker, PECAM-1 as used previously (Somers *et al*., 2012; Somers *et al.,* 2016), confirmed a significantly decreased expression in SMA heart at an early-symptomatic age (P5) (P1: ns > 0.05; P3: ns > 0.05; P5: *< 0.05) (Fig. 5C). This decrease in heart wall microvasculature was particularly apparent at high magnification in the wall immediately adjacent to the ventricular lumen (Fig 5B). This early contributing factor to cardiac defects, is likely to result in hypoxia of cardiomyocytes, similar to that seen at P5 in the spinal cord of the SMA mouse, and may exacerbate increased cell death.

SMA Hearts are Congested with Blood

The hearts used in this study were not perfused prior to fixation. Therefore, residual blood left in the heart after removal is likely a reflection of functional circulatory conditions. In our initial observations of histologically stained hearts, it was apparent that SMA hearts contained more blood than the controls (Fig 1C). To further examine this increase, we stained RBCs with Ly76 (which labels all cells in the erythrocyte lineage including RBCs). Ly76 marker showed that heart chambers viewed in cross-sections of P5 control hearts have only small amounts of blood, whereas SMA hearts are congested with blood, which is most apparent in the ventricles (Fig 6A). Quantification of Ly76 stain showed a significant (2-3 fold) increase in the RBCs in SMA hearts at both pre- and early-symptomatic ages compared to controls (P1: ns > 0.05; P3: *< 0.05; P5: *< 0.05) (Fig 6B). This is consistent with a model where the structural and molecular defects previously observed impact negatively on heart function, resulting in blood pooling.

Discussion

Here, we show that Taiwanese SMA mouse hearts have thinner muscular walls, with disorganised basement membranes and cardiomyocytes present pre-symptomatically. Cardiomyocytes were decreased in density, likely due to increased apoptosis, at an early-symptomatic age; which is associated with increased oxidative stress from birth, and also decreased microvasculature in the heart at an early symptomatic age. This demonstrates that heart defects are an early and important feature of disease pathogenesis in SMA.

The decrease in IVS and LV wall width described here is consistent with findings from other mouse models, and may be linked to congenital heart defects such as septal defects between both atria and ventricles in SMA patients. IVS thinning was present from 3 days postnatally, suggesting a failure to adapt to the radical pressure changes that occur after birth (Rein *et al.,* 1987). LV wall thinning was observed pre-symptomatically at birth, likely affecting heart function and therefore systemic blood flow. Taken together, these findings point toward impaired development of the SMA heart as a significant contributor to cardiovascular defects.

Enlarged ventricles contribute to heart dysfunction in SMA hearts

Enlargement of the ventricles is commonly linked to dilation and dysfunction of the heart, particularly in combination with thinning of the heart walls (Redfield *et al.,* 2003). This is consistent with the cardiac phenotype described here in SMA, where dilation of the ventricles is a secondary event, occurring at P3 after the primary event of a decrease in LV wall width at P1. This dilation phenotype correlates with previous studies showing a decreased ejection fraction in mouse SMA hearts (Bevan *et al.,* 2010; Bogdanik *et al.,* 2015), and with cardiac defects, including dilation of atria and ventricles, diastolic dysfunction and ventricular overload seen in SMA patients (Collado-Oritz et al., 2007; Tanaka et al., 1976; Kimura et al., 1980; Distefano et al., 1994; Elkohen et al., 1996; Finsterer et al., 1999; Menke et al., 2008; Kuru et al., 2009; Grotto et al., 2016). Taken together, thinning of the walls and enlargement of the ventricles in the SMA heart is strikingly similar to dilated cardiomyopathy (DCM), where the heart becomes enlarged and cannot pump blood efficiently, evidenced by blood pooling. These defects will likely result in systolic heart failure (Maron *et al.,* 2006), which has been reported in some SMA patients (Collado-Oritz et al., 2007).

Cardiomyocytes are disorganised in SMA hearts

Our findings suggest that gross abnormalities in the SMA heart are underpinned by cellular defects, likely driven by SMN depletion in the cardiomyocytes. Collagen IV levels were decreased in SMA, likely affecting cardiomyocyte organisation through its role in basement membrane structure (Lundgren *et al.,* 1988). The basement membrane maintains cardiomyocyte shape (Lundgren *et al.,* 1988); anchors them to the ECM (Zellner *et al.,* 1991); regulates their electrical properties (Frank *et al.,* 1977; Yang *et al.,* 2014); regulates sarcomeric formation and remodelling (Ross and Borg, 2001; Yang *et al.,* 2015) and

influences force production (Factor and Robinson, 1988; Yang *et al.,* 2015). Specifically, the collagen IV network increases rigidity and strength resulting in a more fluid and powerful contraction (Bruggink *et al.,* 2007).

This defective basement membrane and abnormal organisation of cardiomyocytes will likely impair electrical conduction through end to end gap junctions (Zellner *et al.,* 1991), preventing a coherent contraction to flow through the heart (Greenbaum *et al.,* 1981; Sedmera and McQuinn, 2009). In addition, trabeculae are more common in SMA hearts and the cardiac muscle is circumferentially rather than spirally oriented, both of which suggest that the heart wall is not maturing correctly in the embryonic period. Compaction of trabeculae contributes to the thickness of the ventricular and IVS muscular mass, the papillary muscles, vasculature and the conduction system (Sedmera *et al.*, 2000). The failed compaction seen in the SMA heart may underlie septal defects and arrhythmias seen in SMA patients.

Oxidative stress is present in SMA hearts

In parallel with the structural defects described above, the pre-symptomatic increases in AT-1 and MT-ATP6 reported here suggest that oxidative stress is present in the SMA heart, and that it precedes increased cardiomyocyte death. Oxidative stress is thought to be critical for the activation of apoptosis, including caspase activation, in failing hearts (Cesselli *et al.,* 2001). AT-1 is also increased in the heart of the Δ7 SMA mouse model (Shababi *et al.,* 2010), which points to oxidative stress as a common mechanism in SMA cardiovascular pathology. In our study caspase levels do not correlate perfectly with cardiomyocyte density, which is likely due to the high variability in proliferation of cardiomyocytes, particularly at P3, contributing to the decrease in cell number prior to the increase in cell death.

As ATP synthase subunits interact directly with SMN protein, and are overexpressed in the CNS of multiple SMA models, there is a potentially direct mechanistic link between SMN depletion and cardiac dysfunction (Fuller *et al.* 2016). Taken further, defects in mitochondria, including fragmentation of the mitochondrial network, impaired mitochondrial membrane potential and increased oxidative stress are all thought to be associated with motor neurone cell death in SMA (Acsadi *et al.,* 2009; Ripolone *et al.,* 2015; Miller *et al.,* 2016; Xu *et al.,* 2016; Boyd *et al.,* 2017). Cardiomyocytes contain many mitochondria (more than skeletal muscle) to support their high-energy demands (Hom and Sheu, 2009), and are therefore highly susceptible to mitochondrial dysfunction-mediated oxidative stress. Swollen and degenerating mitochondria are seen in cardiomyocytes in late-symptomatic SMNΔ7 mice (Bevan *et al.,* 2010), which is consistent with late-stage heart failure. Here, however, we show that the changes in the level of a mitochondrial specific protein, MT-ATP6 are already present at birth suggesting that mitochondrial dysfunction may be a primary driver of cardiac defects in SMA.

Blood pools in the ventricls of SMA hearts

The thin heart walls in SMA are likely to contract less efficiently, resulting in a decreased ejection fraction (Bevan *et al.,* 2010; Bogdanik *et al.,* 2015), blood pooling (Ghio *et al.,* 2001), additional stress, increased cell death and a positive feedback loop ultimately leading to heart failure (Narula *et al.,* 1996). However, the heart is a dynamic organ and abnormal blood flow through the heart, altered by forces including preload and afterload (Bugge-Asperheim and Kiil, 1973), could also contribute to blood pooling. In addition, extrinsic factors such as altered blood composition, including that resulting from abnormal erythropoiesis and platelet production in the SMA liver (Szunyogova *et al.,* 2016), will impact on blood flow and contribute to ventricular distension. These alterations in blood flow and observations of blood pooling could also explain the pulmonary hypertension and pulmonary effusion reported in SMA patients (Møller et al., 1990; Distefano et al., 1994; El-Matary et al., 2004; Menke et al., 2008). Here (see Fig. 7), we propose a model to interpret the cardiac defects observed.

With a new treatment for SMA, Spinraza (Nusinersen), approved by the FDA and EMA, it is now critically important to understand these cardiovascular pathologies. The drug is administered intrathecally, and therefore only targets the central nervous system (Hoy *et al.,* 2017), which appears to limit its utility in disease treatment (Finkel et al., 2017). Conversely, an as yet unapproved, systemically-administered gene therapy, may offer hope of obtaining significant patient benefit (Mendell et al, 2017), by treating the disease as a whole. Consequently, it is an unfortunate possibility that cardiovascular defects may be uncovered in these treated SMA patients.

Conclusion

In conclusion, the severe Taiwanese SMA mouse model has severe cardiac defects from birth. Thinning of the IVS and dilation of ventricular lumens was seen from pre-symptomatic ages through until late symptomatic stages of disease. But most significantly, changes in the LV width were observed from birth, prior to motor neurone pathology. There were also changes in the organisation of cardiomyocytes from birth in SMA, which may be linked to altered levels of basement membrane protein collagen IV; increased oxidative stress in cardiomyocytes pre-symptomatically; increased apoptosis of cardiomyocytes seen at early-symptomatic ages; decreased microvasculature also at an early symptomatic age; and increased blood pooling within the SMA heart ventricles at a pre-symptomatic age. This combines to suggest a phenotype similar to dilated cardiomyopathy that will most likely lead to heart failure. It is therefore essential to develop systemic therapies for SMA capable of treating these cardiac pathologies, in addition to the well-established neuromuscular defects.

Acknowledgements

We would like to acknowledge the Microscopy and Histology Core Facility at the University of Aberdeen, Kevin Mackenzie, Debbie Wilkinson, Gillian Milne and Lucy Wight, for the use of their facilities.
GKM was funded by a research award from RGA awarded to SHP.
ES was funded by a University of Aberdeen Elphinstone PhD Studentship and a research award from the Euan Macdonald Centre for Motor Neurone Disease Research.
HKS was funded by a Euan Macdonald Centre for Motor Neurone Disease Research PhD Studentship.
SHP is funded by Tenovus (Scotland), SMA Trust and Prinses Beatrix Spierfonds.
THG is funded by SMA Trust (UK SMA Research Consortium Award), Muscular Dystrophy UK, and Anatomical Society (PhD Studentship).

Conflict of Interest

Please note that SHP is a member of the JoA Editorial Board and THG is joint EiC of JoA.

Author Contributions

SHP, THG, GKM and ES designed the study
GKM, ES and HKS carried out the experiments
GKM analysed the data
SHP, THG, GKM, ES and HKS prepared the manuscript

References

Acsadi, G., Lee, I., Li, X., Khaidakov, M., Pecinova, A., Parker, G. and Hüttemann, M. (2009). Mitochondrial dysfunction in a neural cell model of spinal muscular atrophy. *Journal of Neuroscience Research,* **87**(12), 2748-2756.

Adachi, S., Ito, H., Tamamori-Adachi, M., Ono, Y., Nozato, T., Abe, S., Ikeda, M., Marumo, F. and Hiroe, M. (2001). Cyclin A/cdk2 activation is involved in hypoxia-induced apoptosis in cardiomyocytes. *Circulation Reseasrch,* **89**(4), 408-414.

Arai, H., Tanabe, Y., Hachiya, Y., Otsuka, E., Kumada, S., Furushima, W., Kohyama, J., Yamashita, S., Takanashi, J. and Kohno, Y. (2005). Finger cold-induced vasodilation, sympathetic skin response and R-R interval variation in patients with progressive spinal muscular atrophy. *Journal of Child Neurology*, **20**(11), 871-875.

Araujo, A., Araujo, M. and Swoboda, K. (2009). Vascular perfusion abnormalities in infants with spinal muscular atrophy. *Journal of Pediatrics*, **155**(2), 292-294.

Bevan, A., Hutchinson, K., Foust, K., Braun, L., McGovern, V., Schmelzer, L., Ward, J., Petruska, J., Lucchesi, P., Burghes, A. and Kasper, B. (2010). Early heart failure in the SMN Δ7 model of spinal muscular atrophy and correction by postnatal scAAV9-SMN delivery. *Human Molecular Genetics,* **19**(20), 3895-3905.

Biondi, O., Lopes, P., Desseille, C., Branchu, J., Chali, F., Salah, A., Pariset, C., Chanoine, C. and Charbonnier, F. (2012). Physical exercise reduces cardiac defects in type 2 spinal muscular atophy-like mice. *Journal of Physiology,* **590**(22), 5907-5925.

Bogdanik, L., Osborne, M., Davis, C., Martin, W., Austin, A., Rigo, F., Bennett, C. and Lutz, C. (2015). Systemic, postsymptomatic antisense oligonucleotide rescues motor unit maturation delay in a new mouse model for type II/III spinal muscular atrophy. *Proceeding of the National Academy of Sciences of the United States of America,* **112**(43), 865-872.

Bowerman, M., Michalski, J., Beauvais, A., Murray, L., De Repentigny, Y. and Kothary, R. (2014). Defects in pancreatic development and glucose metabolism in SMN-depleted mice independent of canonical spinal muscular atrophy neuromuscular pathology. *Human Molecular Genetics,* **23**(13), 3432-3444.

Bowerman, M., Swoboda, K., Michalski, J., Wang, G., Reeks, C., Beauvais, A., Murphy, K., Woulfe, J., Screaton, R., Scott, F. and Kothary, R. (2012). Glucose metabolism and pancreatic defects in spinal muscular atrophy. *Annals of Neurology,* **72**(2), 256-268.

Boyd, P., Tu, W., Shorrock, H., Groen, E., Carter, R., Powis, R., Thomson, S., Thomson, D., Graham, L., Motyl, A., Wishart, T., Highley, J., Morton, N., Becker, T., Becker, C., Heath, P. and Gillingwater, T. (2017). Bioenergetic status modulates motor neuron vulnerability and

pathogenesis in a zebrafish model of spinal muscular atrophy. *PLOS Genetics,* **13**(4), e1006744.

Bruggink, A., Van Oosterhout, M., De Jonge, N., Cleutjens, J., Van Wichen, D., Van Kuik, J., Tilanus, M., Gmelig-Meyling, F., Van Den Tweel, J. and De Wenger, R. (2007). Type IV collagen degradation in the myocardial basement membrane after unloading of the failing heart by a left ventricular assist device. *Laboratory Investigation,* **87**(11), 1125-1137.

Bugge-Asperheim, B. and Kiil, F. (1973). Preload, contractility, and afterload as determinants of stroke volume during elevation of aortic blood pressure in dogs. *Cardiovascular Research,* **7**(4), 328-341.

Buja, M. and Entman, M. (1998). Modes of myocardial cell injury and cell death in ischemic heart disease. *Circulation,* **98**(14), 1355-1357.

Bürglen, L., Spiegel, R., Ignatius, J., Cobben, J., Landrieu, P., Lefebvre, S., Munnich, A. and Melki, J. (1995). SMN gene deletion in variant of infantile spinal muscular atrophy. *The Lancet*, **346**(8970), 316-317.

Catapano, F., Zaharieva, I., Scoto, M., Marrosu, E., Morgan, J., Muntoni, F. and Zhou, H. (2016). Altered levels of microRNA-9, -206, and -132 in spinal muscular atrophy and their response to antisense oligonucleotide therapy. *Molecular Therapy – Nucleic Acids,* **5**(7), e331.

Cesselli, D. Jakoniuk, I., Barlucchi,L., Beltrami, A., Hintze, T., Nadal-Ginard, B., Kajstura, J., Leri, A. and Anversa, P. (2001). Oxidative stress-mediated cardiac cell death is a major determinant of ventricular dysfunction and failure in dog dilated cardiomyopathy. *Circulation Research,* **89**(3), 279-286.

Collado-Ortiz, M., Shkurovich-Bialik, P., González-De Leo, S. ad Arch-Tirado, E. (2007). Type 1 spinal atrophy (Werdnig-Hoffman disease). Case report. *Cirugia y Cirujanos*, **75**(2), 119-122.

Coletta, C., Carboni, P., Carunchio, A., Porro, G. and Bacci, V. (1989). Electrocardiographic abnormalities in childhood spinal muscular atrophy. *International Journal of Cardiology,* **24**(3), 283-288.

Cook, A., Curzon, C. and Milazzo, A. (2006). An infant with hypoplastic left heart syndrome and spinal muscular atrophy. *Cardiology in the Young,* **16**(1), 78-80.

Dawood, A. and Moosa, A. (1983). Hand and ECG tremor in spinal muscular atrophy. *Archives of Disease in Childhood,* **58**(5), 376-378.

Deguise, M., De Repentigny, Y., McFall, E., Auclair, N., Sad, S. and Kothary, R. (2017). Immune dysregulation may contribute to disease pathogenesis in spinal muscular atrophy mice. *Human Molecular Genetics*, **26**(4), 801-819.

602 Distefano, G., Sciacca, P., Parisi, M., Parano, E., Smilari, P., Marietta, M. and Fiumara, A.
603 (1994). Heart involvement in progressive spinal muscular atrophy. A review of the literature
604 and case histories in childhood. *Pediatria Medica Chirurgica*, **16**(2), 125-128.

605 Eaton, S., Hurtado, M., Oldknow, K., Graham, L., Marchant, T., Gillingwater, T., Farquharson,
606 C. and Wishart, T. (2014). A guide to modern quantitative fluorescent western blotting with
607 troubleshooting strategies. *Journal of Visualized Experiments*, **93**, e52099.

608 Eaton, S., Roche, S., Hurtado, M., Oldknow, K., Farquharson, C., Gillingwater, T. and Wishart,
609 T. (2013). Total protein analysis as a reliable loading control for quantitative fluorescent
610 western blotting. *PLOS One*, **8**(8), e72457.

611 El-Matary, W., Kotagiri, S., Cameron, D. and Peart, I. (2004). Spinal muscle atrophy type 1
612 (Werdnig-Hoffman disease) with complex cardiac malformation. *European Journal of*
613 *Pediatrics,* **163**(6), 331-332.

614 Elkohen, M., Vaksmann, G., Elkohen, M., Francart, C., Foucher, C. and Rey, C. (1996). Cardiac
615 involvement in Kugelberg-Welander disease: A prospective study of 8 cases. *Archives des*
616 *Maladies du Coeur et des Vaisseaux,* **89**(5), 611-617.

617 Factor, S. and Robinson, T. (1988). Comparative connective tissue structure-function
618 relationships in biological pumps. *Lab Investigations,* **58**(2), 150-156.

619 Finkel, R., Mercuri, E., Darras, B., Connolly, A., Kuntz, N., Kirschner, J., Chiriboga, C., Saito, K.,
620 Servais, L., Tizzano, E., Topaloglu, H., Tulinius, M., Montes, J., Glanzman, A., Bishop, K.,
621 Zhong, Z., Gheuens, S., Bennett, C., Schneider, E., Farwell, W. and De Vivo, D. (2017).
622 Nusinersen versus sham control in infantile-onset spinal muscular atrophy. *The New*
623 *England Journal of Medicine,* **377**(18), 1723-1732.

624 Finsterer, J. and Stöllberger, C. (1999) Cardiac involvement in Werdnig-Hoffmann's spinal
625 muscular atrophy. *Cardiology,* **92**(3), 178-182.

626 Frank, J., Langer, G., Nudd, L. and Seraydarian, K. (1977). The myocardial cell surface, its
627 histochemistry, and the effect of sialic acid and calcium removal on its structure and cellular
628 ionic exchange. *Circulation Research,* **41**(5), 702-714.

629 Fuller, H., Gillingwater, T. and Wishart, T. (2016). Commonality amid diversity: Multi-study
630 proteomic identification of conserved disease mechanisms in spinal muscular atrophy.
631 *Neuromuscular Disorders,* **26**(9), 560-569.

632 Gardner-Medwin, D., Hudgson, P. and Walton, J. (1967). Benign spinal muscular atrophy
633 arising in childhood and adolescence. *Journal of the Neurological Sciences,* **5**(1), 121-158.

634 Ghio, S., Gavazzi, A., Campana, C., Inserra, C., Klersy, C., Sebastiani, R., Arbustini, E.,
635 Recusani, F. and Tavazzi, L. (2001). Independent and additive prognostic value of right

636 ventricular systolic function and pulmonary artery pressure in patients with chronic heart
637 failure. *Journal of the American College of Cardiology,* **37**(1), 183-188.

638 Gogliotti, R., Quinlan, K., Barlow, C., Heier, C., Heckman, C. and DiDonato, C. (2012). Motor
639 neuron rescue in spinal muscular atrophy mice demonstrates that sensory-motor defects
640 are a consequence, not a cause, of motor neuron dysfunction. *Journal of Neuroscience,*
641 **32**(11), 3818-3829.

642 Greenbaum, R., Ho, S., Gibson, D., Becker, A. and Anderson, R. (1981). Left ventricular fibre
643 architecture in man. *British Heart Journal,* **45**(3), 248-263.

644 Grotto, S., Cuisset, J., Marret, S., Drunat, S., Faure, P., Audebert-Bellanger, S., Desguerre,
645 I., Flurin, V., Grebille, A., Guerrot, A., Journel, H., Morin, G., Plessis, G., Renolleau, S., Roume,
646 J., Simon-Bouy, B., Touraine, R., Willems, M., Frébourg, T., Verspyck, E., Saugier-Veber, P.
647 (2016). Type 0 spinal muscular atrophy: Further delineation of prenatal and postnatal
648 features in 16 patients. *Journal of Neuromuscular Diseases*, **3**(4), 487-495.

649 Hachiya, Y., Arai, H., Hayashi, M., Kumada, S., Furushima, W., Ohtsuka, E., Ito, Y., Uchiyama,
650 A. and Kurata, K. (2005). Autonomic dysfunction in cases of spinal muscular atrophy type 1
651 with long survival. *Brain and Development,* **27**(8), 574-578.

652 Haliloglu, G., Gungor, M. and Anlar, B. (2015). The role of electrocardiography in the
653 diagnosis of spinal muscular atrophy type III. *The Journal of Pediatrics,* **166**(4), 1092.

654 Hamilton, G. and Gillingwater, T. (2013). Spinal muscular atrophy: Going beyond the motor
655 neuron. *Trends in Molecular Medicine,* **19**(1), 40-50.
656
657 Heier, C., Satta, R., Lutz, C. and Didonato, C. (2010). Arrhythmia and cardiac defects are a
658 feature of spinal muscular atrophy model mice. *Human Molecular Genetics,* **19**(20), 3906-
659 3918.

660 Hoffmann, J. (1892). Familial spinal muscular atrophy in infancy. *Dtsch Z Nervenheilkd,* **3**,
661 427-470.

662 Hom, J., Sheu, S. (2009). Morphological dynamics of mitochondria – A special emphasis on
663 cardiac muscle cells. *Journal of Molecular and Cellular Cardiology,* **46**(6), 811-820.

664 Hoy, S. (2017). Nusinersen: First global approval. *Drugs,* **77**(4), 473-479.

665 Hsieh-Li, H., Chang, J., Jong, Y., Wu, M., Wang, N., Tsai, C. and Li, H. (2000). A mouse model
666 for spinal muscular atrophy. *Nature Genetics,* **24**(1), 66-70.

667 Hua, Y., Liu, Y., Sahashi, K., Rigo, F., Bennett, C. and Krainer, A. (2015) Motor neuron cell-
668 nonautonomous rescue of spinal muscular atrophy phenotypes in mild and severe
669 transgenic mouse models. *Genes and Development,* **29**(3), 288-297.

Hua, Y., Sahashi, K., Rigo, F., Hung, G., Horev, G., Bennett, C. and Krainer, A. (2011). Peripheral SMN restoration is essential for long-term rescue of a severe spinal muscular atrophy mouse model. *Nature*, **478**(7367), 123-126.

Jonckheere, A., Smeitink, J. and Rodenburg, R. (2012). Mitochondrial ATP synthase: Architecture, function and pathology. *Journal of Inherited Metabolic Disease,* **35**(2), 211-225.

Jong, Y., Chang, J. and Wu, J. (1998). Large-scale deletions in a Chinese infant associated with a variant form of Werdnig-Hoffmann disease. *Neurology*, **51**(3), 878-879.

Khairallah, M., Astroski, J., Custer, S., Androphy, E., Franklin, C. and Lorson, C. (2017). SMN deficiency negatively impacts red pulp macrophages and spleen development in mouse models of spinal muscular atrophy. *Human Molecular Genetics*, **26**(5), 932-941.

Kimura, S., Yokota, H., Tateda, K., Miyamoto, K., Yamamoto, K., Shibata, J. (1980). A case of the Kugelberg-Welander syndrome complicated with cardiac lesions. *Japanese Heart Journal,* **21**(3), 417-422.

Krupickova, S., Rigby, M., Jicinska, H., Marais, G., Rubens, M. and Carvalho, J. (2017). Total anomalous pulmonary venous connection to an unroofed coronary sinus diagnosed in a fetus with associated spinal muscular atrophy type I. *Ultrasound in Obstetrics and Gynecology,* uog. 17432**.**

Kuru, S., Sakai, M., Konagaya, M., Yoshida, M., Hashizume, Y. and Saito, K. (2009). An autopsy case of spinal muscular atrophy type III (Kugelberg-Welander disease). *Neuropathology,* **29**(1), 63-67.

Lefebvre, S., Bürglen, L., Reboullet, S., Clermont, O., Burlet, P., Viollet, L., Benichou, B., Cruaud, C., Millasseau, P., Zeviani, M., Le Paslier, D., Frézal, J., Cohen, D., Weissenbach, J., Munnich, A. and Melki. (1995). Identification and characterisation of a spinal muscular atrophy-determining gene. *Cell,* **80**(1), 155-156.

Lorson, C., Hahnen, E., Androphy, E. and Wirth, B. (1999). A single nucleotide in the SMN gene regulates splicing and is responsible for spinal muscular atrophy. *Proceedings of the National Academy of Sciences*, **96**(11), 6307-6311.

Lundgren, E., Gullberg, D., Rubin, K., Borg, T., Terracio, M. and Terracio, L. (1988). In vitro studies on adult cardiac myocytes: Attachment and biosynthesis of collagen IV and laminin. *Journal of Cellular Physiology,* **136**(1), 43-53.

Lunn, M. and Wang, C. (2008). Spinal muscular atrophy. *The Lancet,* **371**(9630), 2120-2133.

Manczak, M., Jung, Y., Park, B., Partovi, D. and Reddy, P. (2005). Time-course of mitochondrial gene expressions in mice brains: implications for mitochondrial dysfunction, oxidative damage, and cytochrome c in aging. *Journal of Neurochemistry,* **92**(3), 494-504.

Maron, B., Towbin, J. Thiene, G., Antzelevitch, C., Corrado, D., Arnett, D., Moss, A., Seidman, C. and Young, J. (2006). An American Heart Association scientific statement from the council on clinical cardiology, heart failure and transplantation committee; quality of care and outcomes research and functional genomics and translational biology interdisciplinary working groups; and council on epidemiology and prevention. *Circulation,* **113**(14), 1807-1816.

Martínez-Reyes, I. and Cuezva, J. (2014). The H^+-ATP synthase: A gate to ROS-mediated cell death or cell survival. *Biochimica et Biophysica Acta – Bioenergetics,* **1837**(7), 1099-1112.

Mendell, J., Al-Zaidy, S., Shell, R., Arnold, W., Rodino-Klapac, L., Prior, T., Lowes, L., Alfano, L., Berry, K., Church, K., Kissel, J., Nagendran, S., L'Italien, J., Sproule, D., Wells, C., Cardenas, J., Heitzer, M., Kaspar, A., Corcoran, S., Braun, L., Likhite, S., Miranda, C., Meyer, K., Foust, K., Burghes, A. and Kaspar, B. (2017). Single-dose gene-replacement therapy for spinal muscular atrophy. *The New England Journal of Medicine,* **377**(18), 1713-1722.

Menke, L., Poll-The, B., Clur, S., Bilardo, C., Van Der Wal, A., Lemmink, H. and Cobben, J. (2008). Congenital heart defects in spinal muscular atrophy type I: A clinical report of two siblings and a review of the literature. *American Journal of Medical Genetics, Part A,* **146**(6), 740-744.

Miller, N., Shi, H., Zelikovich, A. and Ma, Y. (2015). Motor neuron mitochondrial dysfunction in spinal muscular atrophy. *Human Molecular Genetics,* **25**(16), 3395-3406.

Møller, P., Moe, N., Saugstad, O., Skullerud, K., Velken, M., Berg K, Nitter-Hauge, S and Børresen, A. (1990) Spinal muscular atrophy type 1 combined with atrial septal defect in three sibs. *Clinical Genetics*. **38**(2), 81-83.

Mulleners, W., Van Ravenswaay, C., Gabreels, F., Hamel, B., Van Oort, A. and Sengers, R. (1996). Spinal muscular atrophy combined with congenital heart disease: A report of two cases. *Neuropediatrics,* **27**(6), 333-334.

Narula, J., Haider, N., Virmani, R., Disalvo, T., Kolodgie, F., Hajjar, R., Schmidt, U., Semigran, M., Dec, G. and Khaw, B. (1996). Apoptosis in myocytes in end-stage heart failure. *New England Journal of Medicine,* **335**(16), 1182-1189.

Narver, H., Kong, L., Burnett, B., Choe, D., Bosch-Marcé, M., Taye, A., Eckhaus, M. and Sumner, C. (2008). Sustained improvement of spinal muscular atrophy mice treated with trichostatin A plus nutrition. *Annals of Neurology,* **64**(4), 465-470.

Nash, L., Burns, J., Chardon, J., Kothary, R. and Parks, R. (2016). Spinal muscular atrophy: More than a disease of motor neurons? *Current Molecular Medicine,* **16**(9), 779-792.

739 Ottesen, E., Howell, M., Singh, N., Seo, J., Whitley, E. and Singh, R. (2016). Severe
740 impairment of male reproductive organ development in a low SMN expressing mouse
741 model of spinal muscular atrophy. *Scientific Reports,* **6**, 20193.

742 Porter, A. and Jänicke, R. (1999) Emerging roles of caspase-3 in apoptosis. *Cell Death and*
743 *Differentiation,* **6**(2), 99-104.

744 Powis, R. and Gillingwater, T. (2016a). Selective loss of alpha motor neurons with sparing of
745 gamma motor neurons and spinal cord cholinergic neurons in a mouse model of spinal
746 muscular atrophy. *Journal of Anatomy,* **228**(3), 443-451.

747 Powis, R., Karyka, E., Boyd, P., Côme, J., Jones, R., Zheng, Y., Szunyogova, E., Groen, E.,
748 Hunter, G., Thomson, D., Wishart, T., Becker, C., Parson, S., Martinat, C., Azzouz, M. and
749 Gillingwater, T. (2016b). Systemic restoration of UBA1 ameliorates disease in spinal
750 muscular atrophy. *JCI Insight,* **1**(11), e87908.

751 Qin, F., Patel, R., Yan, C. and Weimin, L. (2005). NADPH oxidase is involved in angiotensin II-
752 induced apoptosis in H9C2 cardiac muscle cells: Effects of apocynin. *Free Radical Biology*
753 *and Medicine,* **40**(2), 236-246.

754 Redfield, M., Jacobsen, S., Burnett, J., Mahoney, D., Bailey, K. and Rodeheffer, R. (2003).
755 Burden of systolic and diastolic ventricular dysfunction in the community: Appreciating the
756 scope of the heat failure epidemic. *Journal of the American Medical Association,* **289**(2),
757 194-202.

758 Rein, A., Sanders, S., Colan, S., Parness, I. and Epstein, M. (1987). Left ventricular mechanics
759 in the normal newborn. *Circulation,* **76**(5), 1029-1036.

760 Riessland, M., Ackermann, B., Förster, A., Jakubik, M., Hauke, J., Garbes, L., Fritzsche, I.,
761 Mende, Y., Blumcke, I., Hahnen, W. and Wirth, B. (2010). SAHA ameliorates the SMA
762 phenotype in two mouse models for spinal muscular atrophy. *Human Molecular Genetics,*
763 **19**(8), 1492-1506.

764 Ripolone, M., Ronchi, D., Violano, R., Vallejo, D., Fagiolari, G., Barca, E., Lucchini, V.,
765 Colombo, I., Villa, L., Berardinelli, A., Balottin, U., Morandi, L., Mora, M., Bordoni, A.,
766 Fortunato, F., Corti, S., Parisi, D., Toscano, A., Sciacco, M., Di Mauro, S.,, Comi, G. and
767 Moggio, M. (2015). Impaired muscle mitochondrial biogenesis and myogenesis in spinal
768 muscular atrophy. *JAMA Neurology*, **72**(6), 666-675.
769
770 Roos, M., Sarkozy, A., Chierchia, G., De Wilde, P., Schmedding, E. and Brugada, P. (2009).
771 Malignant ventricular arrhythmia in a case of adult onset of spinal muscular atrophy
772 (Kugelberg-Welander disease). *Journal of Cardiovascular Electrophysiology,* **20**(3), 342-344.
773

774 Ross, R. and Borg, T. (2001). Integrins and the myocardium. *Circulation Research,* **88**(11),
775 1112-1119.

776 Rudnik-Schöneborn, S., Heller, R., Berg, C., Betzler, C., Grimm, T., Eggermann, T.,
777 Eggermann, K., Wirth, R., Wirth, B. and Zerres, K. (2008). Congenital heart disease is a
778 feature of severe infantile spinal muscular atrophy. *Journal of Medical Genetics*, **45**(10), 635-
779 638.

780 Rudnik-Schöneborn, S., Vogelgesang, S., Armbrust, S., Graul-Neumann, L., Fusch, C. and
781 Zerres, K. (2010). Digital necroses and vascular thrombosis in severe spinal muscular
782 atrophy. *Muscle and Nerve,* **42**(1), 144-147.

783 Sarnat, H. and Trevenen, C. (2007). Motor neuron degeneration in a 20-week male fetus:
784 spinal muscular atrophy type 0. *Canadian Journal of Neurological Sciences,* **34**(2), 215-220.

785 Scholzen, T. and Gerdes, J. (2000). The Ki-67 protein: From the known and the unknown.
786 *Journal of Cellular Physiology,* **182**(3), 311-322.

787 Schreml, J., Riessland, M., Paterno, M., Garbes, L., Roßbach, K., Ackermann, B., Krämer,
788 J., Somers, E., Parson, S., Heller, R., Berkessel, A., Sterner-Kock, A. and Wirth, B. (2013).
789 Severe SMA mice show organ impairment that cannot be rescued by therapy with the
790 HDACi JNJ-26481585. *European Journal of Human Genetics,* **21**(6), 643-652.

791 Sedmera, D. and McQuinn, T. (2008). Embryogenesis of the heart muscle. *Heart Failure*
792 *Clinics,* **4**(3), 235-245.

793 Sedmera, D., Pexieder, T., Vuillemin, M., Thompson, R. and Anderson, R. (2000).
794 Developmental patterning of the myocardium. *Anatomical Record,* **258**(4), 319-337.

795 Shababi, M., Habibi, J., Ma, L., Glascock, J., Sowers, J. and Lorson, C. (2012). Partial
796 restoration of cardio-vascular defects in a rescued severe model of spinal muscular atrophy.
797 *Journal of Molecular and Cellular Cardiology*, **52**(5), 1074-1082.

798 Shababi, M., Habibi, J., Yang, H., Vale, S., Sewell, W. and Lorson, C. (2010). Cardiac defects
799 contribute to the pathology of spinal muscular atrophy models. *Human Molecular Genetics,*
800 **19**(20), 4059-4071.

801 Shababi, M., Lorson, C. and Rudnik-Schöneborn, S. (2014). Spinal muscular atrophy: a motor
802 neuron disorder or a multi-organ disease? *Journal of Anatomy*, **224**(1), 15-28.
803
804 Sintusek, P., Catapano, F., Angkathunkayul, N., Marrosu, E., Parson, S., Morgan, J., Muntoni,
805 F. and Zhou, H. (2016). Histopathological defects in intestine in severe spinal muscular
806 atrophy mice are improved by systemic antisense oligonucleotide treatment. *PLOS One,*
807 **11**(5), e0155032.

808 Somers, E., Lees, R., Hoban, K., Sleigh, J., Zhou, H., Muntoni, F., Talbot, K., Gillingwater, T.
809 and Parson, S. (2016). Vascular defects and spinal cord hypoxia in spinal muscular atrophy.
810 *Annals of Neurology,* **79**(2), 217-230.

811 Somers, E., Stencel, Z., Wishart, T., Gillingwater, T. and Parson, S. (2012). Density, calibre
812 and ramification of muscle capillaries are altered in a mouse model of severe spinal
813 muscular atrophy. *Neuromuscular Disorders*, **22**(5), 435-442.

814 Sterne, J. and Lavieuville, M. (1964). Cardiac manifestations during diseases of the nervous
815 and muscular systems. *Gazette Médicale de France,* **71**, 1925-1932.

816 Szunyogova, E., Zhou, H., Maxwell, G., Powis, R., Muntoni, F., Gillingwater, T. and Parson, S.
817 (2016). Survival Motor Neuron (SMN) protein is required for normal
818 mouse liver development. *Scientific Reports,* **6**, 34635

819 Takahashi, N., Shimada, T., Ishibashi, Y., Sugamori, T., Hirano, Y., Oyake, N. and Murakami, Y.
820 (2006). Cardiac involvement in Kugelberg-Welander disease: A case report and review.
821 *American Journal of the Medical Sciences,* **332**(6), 354-356.

822 Tanaka, H., Nishi, S., Nuruki, K., Tanaka, N. (1977). Myocardial ultrastructural changes in
823 Kugelberg-Welander syndrome. *British Heart Journal,* **39**(12), 1390-1393.

824 Tanaka, H., Uemura, N., Toyama, Y., Kudo, A. and Ohkatsu. (1976). Cardiac involvement in
825 the Kugelbert-Welander syndrome. *American Journal of Cardiology,* **38**(4), 528-532.

826 Thomson, A., Somers, E., Powis, R., Shorrock, H., Murphy, K., Swoboda, K., Gillingwater, T.
827 and Parson, S. (2016). Survival of motor neuron protein is required for normal postnatal
828 development of the spleen. *Journal of Anatomy,* **230**(2), 337-346.

829 Tsai, M., Chiu, Y., Wang, S., Hsieh-Li, H., Lian, W., Li, H. (2006). Abolishing bax-dependent
830 apoptosis shows beneficial effects on spinal muscular atrophy model mice. *Molecular*
831 *Therapy,* **13**(6), 1149-1155.

832 Vaidla, E., Talvik, I., Kulla, A., Sibul, H., Maasalu, K., Metsvaht, T., Piirsoo, A. and Talvik, T.
833 (2007). Neonatal spinal muscular atrophy type 1 with bone fractures and heart defect.
834 *Journal of Child Neurology,* **22**(1), 67-70.

835 Vitte, J., Davoult, B., Roblot, N., Mayer, M., Joshi, V., Courageot, S., Tronche, F., Vadrot, J.,
836 Moreau, M., Kemeny, F. and Melki, J. (2004). Deletion of murine Smn exon 7 directed to
837 liver leads to severe defect of liver development associated with iron overload. *The*
838 *American Journal of Pathology*, **165**(5), 1731-1741.

839 Werdnig, G. (1891). Two early infantile hereditary cases of progressive muscular atrophy
840 simulating dystrophy, but on a neural basis. *Archives of Psychiatric Nursing,* **22**, 437–481.

Wijngaarde, C., Blank, A., Stam, M., Wadman, R., Van Den Berg, L. and Van Der Pol, W. (2017). Cardiac pathology in spinal muscular atrophy: a systematic review. *Orphanet Journal of Rare Diseases*, **12**(1), 67.

Wishart, T., Mutsaers, X., Riessland, M., Reimer, M., Hunter, G., Hannam, M., Eaton, S., Fuller, H., Roche, S., Somers, E., Morse, R., Young, P., Lamont, D., Hammerschmidt, M., Joshi, A., Hohenstein P., Morris, G., Parson, S., Skehel, P., Becker, T., Robinson, I., Becker, C., Wirth, B. and Gillingwater, T. (2014). Dysregulation of ubiquitin homeostasis and β-catenin signaling promote spinal muscular atrophy. The *Journal of Clinical Investigation*, **124**(4), 1821-1834.

Xu, C., Denton, K., Wang, Z., Zhang, X. and Li, X. Abnormal mitochondrial transport and morphology as early pathological changes in human models of spinal muscular atrophy. *DMM Disease Models and Mechanisms,* **9**(1), 39-49.

Yang, H., Borg, T., Liu, H. and Gao, B. (2015). Interactive relationship between basement-membrane development and sarcomerogenesis in single cardiomyocytes. *Experimental Cell Research,* **330**(1), 222-232.

Yang, H., Borg, T., Wang, Z., Ma, Z. and Gao, B. (2014). Role of the basement membrane in regulation of cardiac electrical properties. *Annals of Biomedical Engineering,* **42**(6), 1148-1157.

Zellner, J., Spinale, F., Eble, D., Hewett, K. and Crawford, F. (1991). Alterations in myocyte shape and basement membrane attachment with tachycardia-induced heart failure. *Circulation Research,* **69**(3), 590-600.

Figure Legends

Figure 1:
Gross Morphology of the Heart is Altered in SMA
(A) Representative images of early-symptomatic P5 hearts from heterozygous control and SMA disease mice. Scale bar represents 5mm. **(B)** Weight of control and SMA heart, expressed as as a % of body weight, at birth (P1), pre-symptomatic (P3), early-symptomatic (P5) and late-symptomatic ages (P8). **(C)** Transverse sections through the ventricles of early-symptomatic P5 hearts of control and SMA mice stained with H&E, LV= left ventricle, RV = right ventricle, scale bar represents 200µm. **(D)** Cross-sectional area of both ventricles, expressed as a % of total cross sectional area of heart in control and SMA mice at birth (P1), pre-symptomatic (P3) and early-symptomatic (P5) ages. **(E)** Width of interventricular septum (IVS) in relation to body weight of control and SMA mice at birth (P1), pre-symptomatic (P3) and early-symptomatic (P5) ages. **(F)** Width of LV wall in relation to body weight of control and SMA mice at birth (P1), pre-symptomatic (P3) and early-symptomatic (P5) ages.
Error bars, mean ±SEM (n≥3 mice per group). A two-way ANOVA was used to calculate *p*-values.

Figure 2:
Cardiomyocytes are Disorganised in the SMA Heart
(A) Representative micrographs in control and SMA hearts, at birth (P1), pre-symptomatic (P3) and early-symptomatic (P5) ages, immunostained for collagen IV to show the basement membrane. Images show transverse sections of whole hearts, with basement membrane indicated in white, red lines show the boundary of the compact wall of the heart, and dashed red lines highlight the orientation of cardiac muscle surrounding the left ventricle. Scale bar represents 50µm. **(B)** Representative micrographs of P5 control and SMA mouse hearts immunostained for collagen IV to show the basement membrane. High power representative images of collagen IV (red) and DAPI nuclei (blue) staining of the heart wall of the left ventricle and of trabeculations projecting into the lumen of the left ventricle. Scale bar represents 50µm. **(C)** Quantitative Western blot showing total levels of collagenIV, at birth (P1) in control and SMA hearts. Error bars, mean ±SEM (n≥3 mice per group). Unpaired student two-tailed *t*-test was used to calculate *p*-values.

Figure 3:
SMA Hearts Have a Decreased Number of Cardiomyocytes and an Increase in Apoptosis
(A) Panels show co-immunostaining of nuclei of the cardiomyocytes with DAPI (blue) and Ki67 (red) to indicate dividing cells in control and SMA hearts, at birth (P1), pre-symptomatic (P3) and early-symptomatic (P5) ages, at low (i,ii) and high power (iii,iv). Scale bar represents 50µm. **(B)** Cardiomyocyte cell density, from nuclear counts, expressed per field of view in control and SMA hearts, at birth (P1), pre-symptomatic (P3) and early-symptomatic (P5) ages. **(C)** Dividing cells (Ki67 positive nuclei) expressed as a percentage of the total number of nuclei per field of view in control and SMA hearts, at birth (P1), pre-symptomatic (P3) and early-symptomatic (P5) ages. **(D)** Quantitative Western blot showing total levels of caspase-3 in control and SMA hearts, at birth (P1), pre-symptomatic (P3) and early-symptomatic (P5) ages.
Error bars, mean ±SEM (n≥3 mice per group). Unpaired student two-tailed *t*-test and a two-way ANOVA were used to calculate *p*-values.

Figure 4:
Oxidative Stress is Present in SMA Hearts
(A) Quantitative Western blot showing the total levles of angiotensin II receptor 1 (AT-1) in control and SMA hearts, at birth (P1), pre-symptomatic (P3) and early-symptomatic (P5) ages. **(B)** Quantitative Western blot showing total levels of mitochondrial ATPsynthase FO subunit 6, at birth (P1) in control and SMA hearts.
Error bars, mean ±SEM (n≥3 mice per group). Unpaired student two-tailed *t*-test was used to calculate *p*-values.

Figure 5:
Heart Microvasculature is Significantly Decreased in SMA
(A) Representative micrographs of microvasculature seen in transverse sections of control and SMA hearts, stained with GSL-1, at birth (P1), pre-symptomatic (P3), early symptomatic (P5) and late-symptomatic (P8) ages. White indicates vasculature. Scale bar represents 50µm. **(B)**High power images of microvasculature in the left ventricular wall of P5 control and SMA hearts; showing GSL-1 only (red) (i,ii) and merged with DAPI nuclei (blue) (iii,iv). Scale bar represents 50µm. **(C)** Quantitative Western blot showing total PECAM-1 level in control and SMA hearts, at birth (P1), pre-symptomatic (P3) and early-symptomatic (P5) ages. Error bars, mean ±SEM (n≥3 mice per group). Unpaired student two-tailed *t*-test was used to calculate *p*-values.

Figure 6:
SMA Hearts are Congested with Blood Post-Mortem
(A) Representative micrographs of transverse sections of P5 control and SMA hearts, stained with Ly76 positive cells to indicate RBC and their precursors, at low (a and b) and high power (c and d). Scale bar represents 50µm. **(B)** Quantification of Ly76 positive cells expressed as a percentage of cross-sectional area of the heart in control and SMA, at birth (P1), pre-symptomatic (P3) and early-symptomatic (P5) ages.
Error bars, mean ±SEM (n≥3 mice per group). A two-way ANOVA was used to calculate *p*-values.

Figure 7:
Proposed Model for Cardiac Defects in SMA

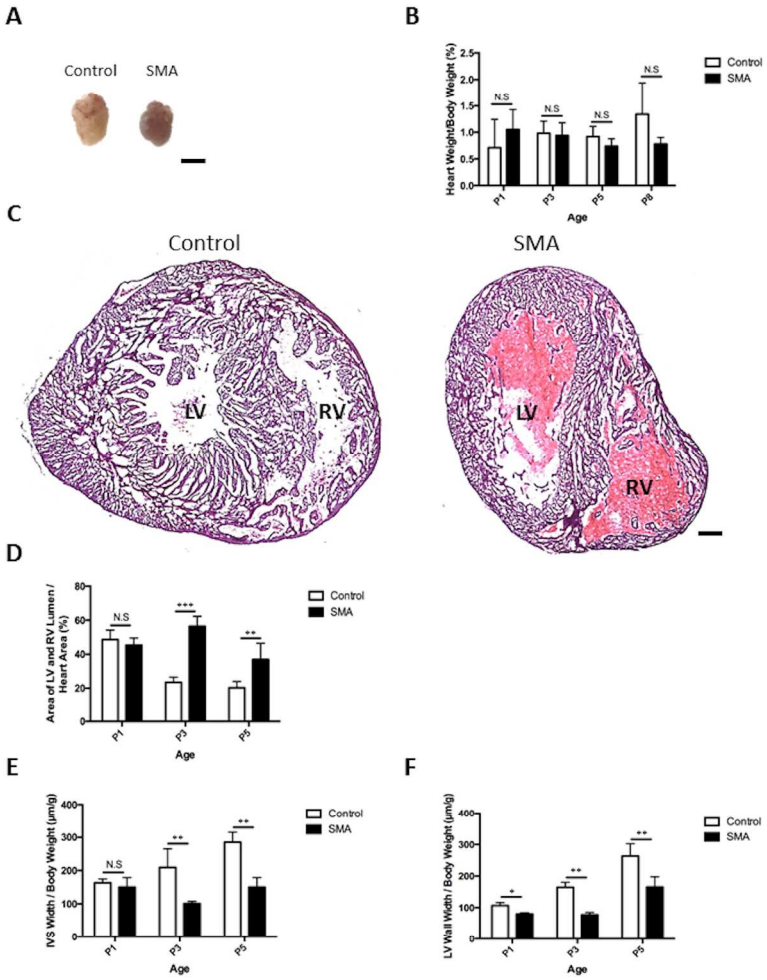

Figure 1:
Gross Morphology of the Heart is Altered in SMA
(A) Representative images of early-symptomatic P5 hearts from heterozygous control and SMA disease mice. Scale bar represents 5mm. (B) Weight of control and SMA heart, expressed as as a % of body weight, at birth (P1), pre-symptomatic (P3), early-symptomatic (P5) and late-symptomatic ages (P8). (C) Transverse sections through the ventricles of early-symptomatic P5 hearts of control and SMA mice stained with H&E, LV= left ventricle, RV = right ventricle, scale bar represents 200µm. (D) Cross-sectional area of both ventricles, expressed as a % of total cross sectional area of heart in control and SMA mice at birth (P1), pre-symptomatic (P3) and early-symptomatic (P5) ages. (E) Width of interventricular septum (IVS) in relation to body weight of control and SMA mice at birth (P1), pre-symptomatic (P3) and early-symptomatic (P5) ages. (F) Width of LV wall in relation to body weight of control and SMA mice at birth (P1), pre-symptomatic (P3) and early-symptomatic (P5) ages.
Error bars, mean ±SEM (n≥3 mice per group). A two-way ANOVA was used to calculate p-values.

190x275mm (300 x 300 DPI)

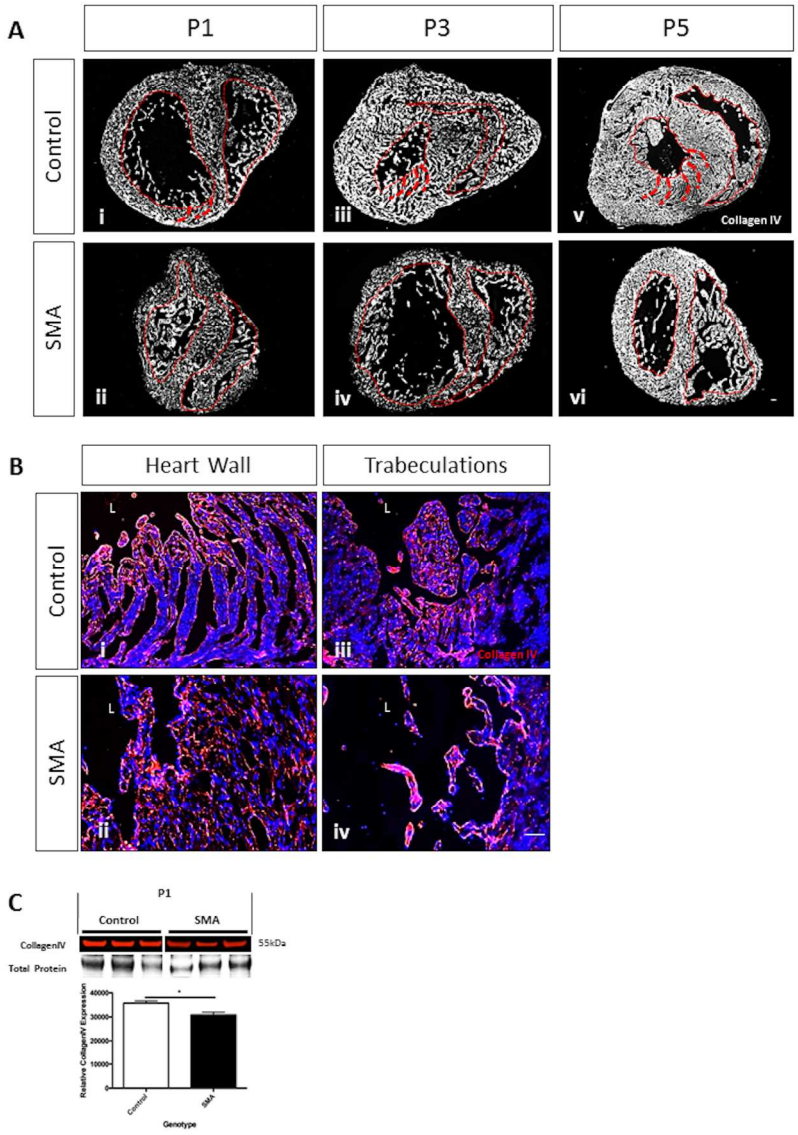

Cardiomyocytes are Disorganised in the SMA Heart

(A) Representative micrographs in control and SMA hearts, at birth (P1), pre-symptomatic (P3) and early-symptomatic (P5) ages, immunostained for collagen IV to show the basement membrane. Images show transverse sections of whole hearts, with basement membrane indicated in white, red lines show the boundary of the compact wall of the heart, and dashed red lines highlight the orientation of cardiac muscle surrounding the left ventricle. Scale bar represents 50μm. (B) Representative micrographs of P5 control and SMA mouse hearts immunostained for collagen IV to show the basement membrane. High power representative images of collagen IV (red) and DAPI nuclei (blue) staining of the heart wall of the left ventricle and of trabeculations projecting into the lumen of the left ventricle. Scale bar represents 50μm. (C) Quantitative Western blot showing total levels of collagenIV, at birth (P1) in control and SMA hearts. Error bars, mean ±SEM (n≥3 mice per group). Unpaired student two-tailed t-test was used to calculate p-values.

190x275mm (300 x 300 DPI)

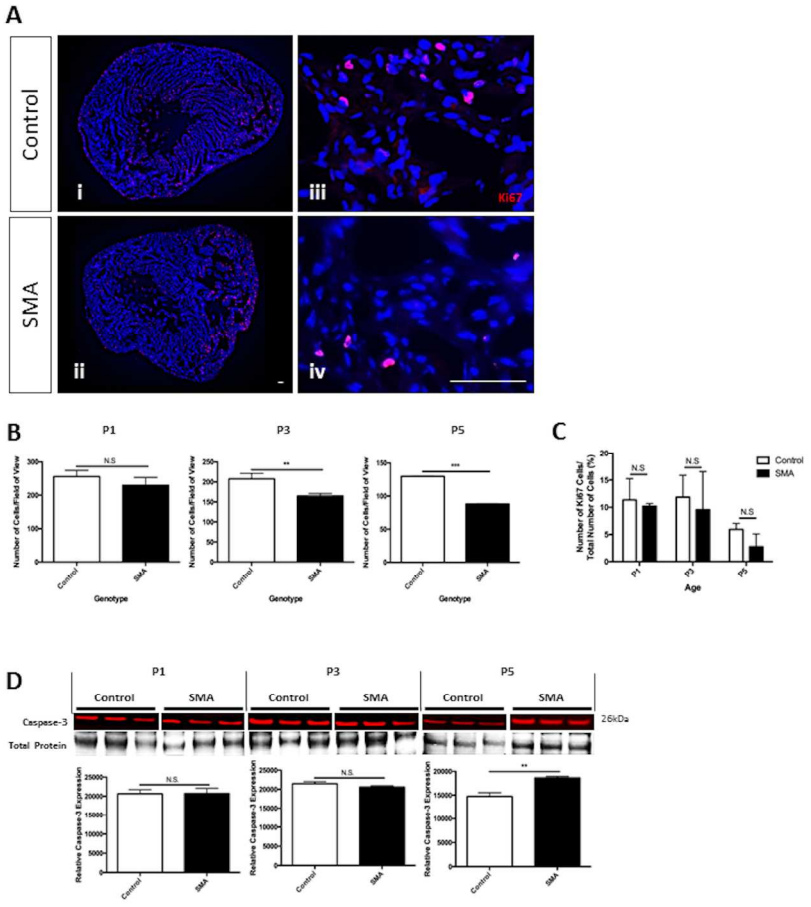

SMA Hearts Have a Decreased Number of Cardiomyocytes and an Increase in Apoptosis
(A) Panels show co-immunostaining of nuclei of the cardiomyocytes with DAPI (blue) and Ki67 (red) to indicate dividing cells in control and SMA hearts, at birth (P1), pre-symptomatic (P3) and early-symptomatic (P5) ages, at low (i,ii) and high power (iii,iv). Scale bar represents 50μm. (B) Cardiomyocyte cell density, from nuclear counts, expressed per field of view in control and SMA hearts, at birth (P1), pre-symptomatic (P3) and early-symptomatic (P5) ages. (C) Dividing cells (Ki67 positive nuclei) expressed as a percentage of the total number of nuclei per field of view in control and SMA hearts, at birth (P1), pre-symptomatic (P3) and early-symptomatic (P5) ages. (D) Quantitative Western blot showing total levels of caspase-3 in control and SMA hearts, at birth (P1), pre-symptomatic (P3) and early-symptomatic (P5) ages.
Error bars, mean ±SEM (n≥3 mice per group). Unpaired student two-tailed t-test and a two-way ANOVA were used to calculate p-values.

190x275mm (300 x 300 DPI)

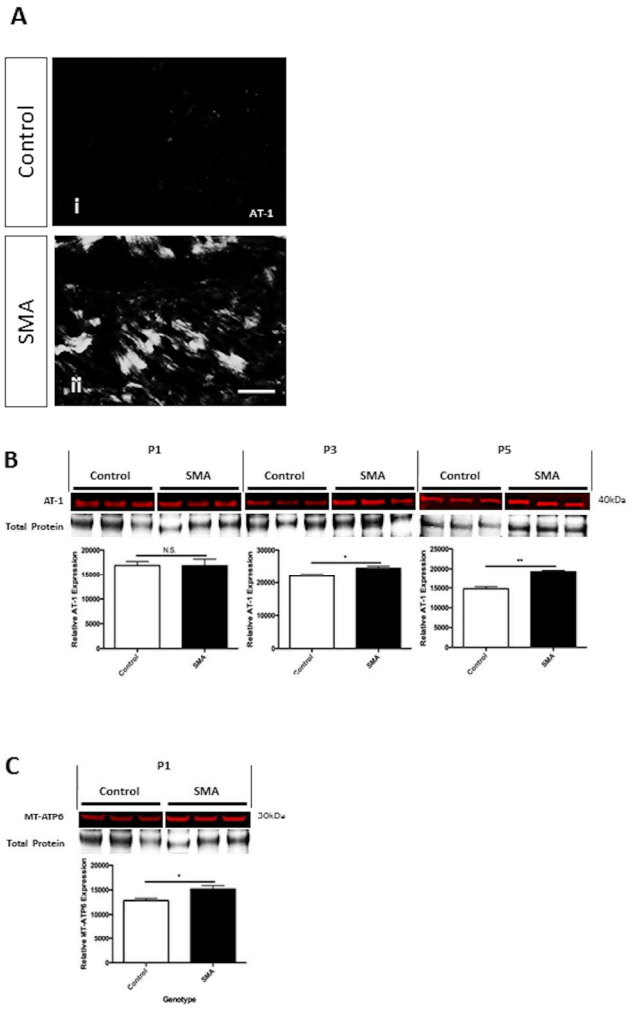

Oxidative Stress is Present in SMA Hearts
(A) Quantitative Western blot showing the total levles of angiotensin II receptor 1 (AT-1) in control and SMA hearts, at birth (P1), pre-symptomatic (P3) and early-symptomatic (P5) ages. (B) Quantitative Western blot showing total levels of mitochondrial ATPsynthase FO subunit 6, at birth (P1) in control and SMA hearts. Error bars, mean ±SEM (n≥3 mice per group). Unpaired student two-tailed t-test was used to calculate p-values.

190x275mm (300 x 300 DPI)

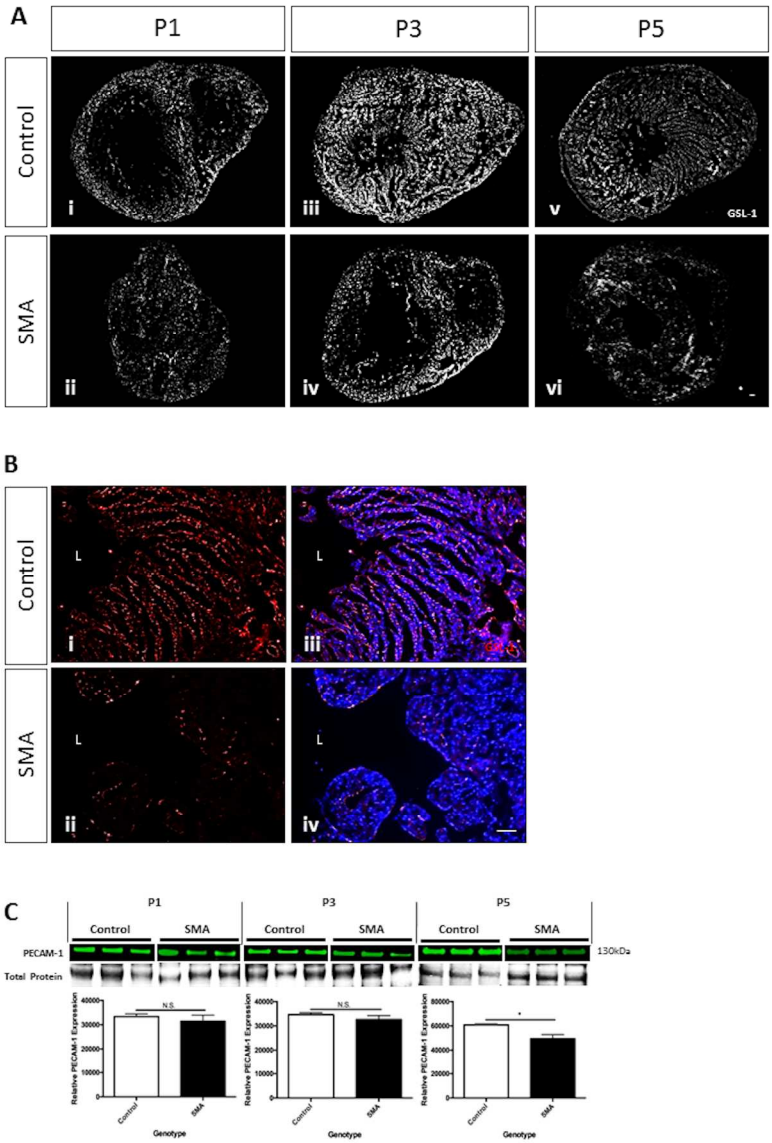

Heart Microvasculature is Significantly Decreased in SMA

(A) Representative micrographs of microvasculature seen in transverse sections of control and SMA hearts, stained with GSL-1, at birth (P1), pre-symptomatic (P3), early symptomatic (P5) and late-symptomatic (P8) ages. White indicates vasculature. Scale bar represents 50μm. (B)High power images of microvasculature in the left ventricular wall of P5 control and SMA hearts; showing GSL-1 only (red) (i,ii) and merged with DAPI nuclei (blue) (iii,iv). Scale bar represents 50μm. (C) Quantitative Western blot showing total PECAM-1 level in control and SMA hearts, at birth (P1), pre-symptomatic (P3) and early-symptomatic (P5) ages. Error bars, mean ±SEM (n≥3 mice per group). Unpaired student two-tailed t-test was used to calculate p-values.

190x275mm (300 x 300 DPI)

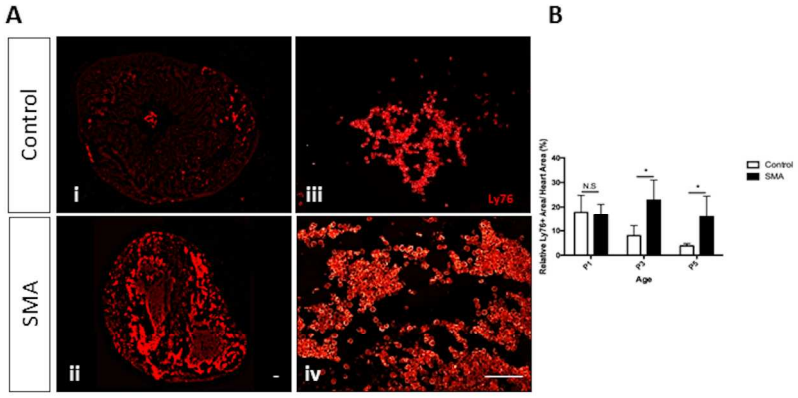

Figure 6:
SMA Hearts are Congested with Blood Post-Mortem
(A) Representative micrographs of transverse sections of P5 control and SMA hearts, stained with Ly76 positive cells to indicate RBC and their precursors, at low (a and b) and high power (c and d). Scale bar represents 50μm. (B) Quantification of Ly76 positive cells expressed as a percentage of cross-sectional area of the heart in control and SMA, at birth (P1), pre-symptomatic (P3) and early-symptomatic (P5) ages. Error bars, mean ±SEM (n≥3 mice per group). A two-way ANOVA was used to calculate p-values.

190x275mm (300 x 300 DPI)

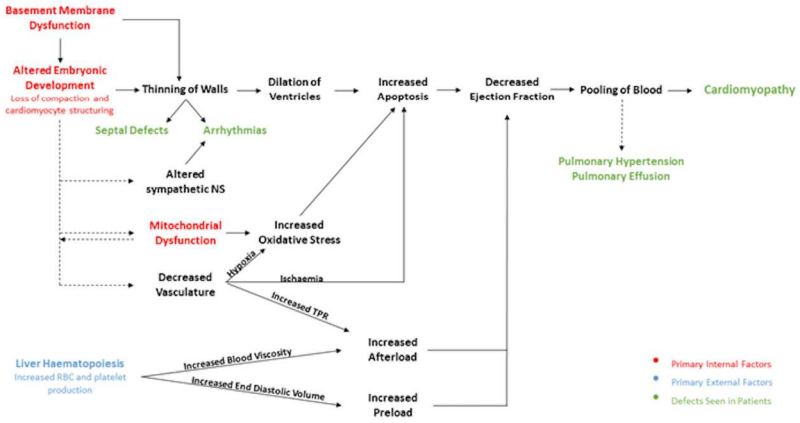

Figure 7:
Proposed Model for Cardiac Defects in SMA

190x275mm (300 x 300 DPI)